

## MINI-REVIEW



# Experimental methods in chemical engineering: Mössbauer spectroscopy

Claudia L. Bianchi<sup>1,2</sup> | Ridha Djellabi<sup>1</sup> | Alessandro Ponti<sup>3</sup> |  
Gregory S. Patience<sup>4</sup>  | Ermelinda Falletta<sup>1,2</sup>

<sup>1</sup>Department of Chemistry, University of Milan, Milan, Italy

<sup>2</sup>Consorzio Interuniversitario Nazionale per la Scienza e Tecnologia dei Materiali (INSTM), Florence, Italy

<sup>3</sup>Istituto di Scienze e Tecnologie Chimiche "Giulio Natta" (SCITEC), Consiglio Nazionale delle Ricerche, Milan, Italy

<sup>4</sup>Chemical Engineering, Polytechnique Montréal, Montréal, Québec, Canada

## Correspondence

Ermelinda Falletta, Department of Chemistry, University of Milan, Milan, Italy.

Email: ermelinda.falletta@unimi.it

## Abstract

When a free nucleus absorbs or emits a gamma ray, it recoils to conserve energy, just like a gun recoils after shooting a bullet. Nuclei bound to a crystal lattice conserve energy when they absorb or emit gamma rays from a nuclear transition as they are fixed so their movement is restricted. This restriction is recoilless nuclear resonance fluorescence—the Mössbauer effect. The energy transmitted through a sample reveals its electronic and molecular structure and magnetic properties but only when the atoms in the source and sample are the same isotope—<sup>57</sup>Co/<sup>57</sup>Fe is the most common couple. So, many of its applications are to identify iron species or how they change as a function of environmental conditions, like corrosion. A bibliometric map identified six major clusters centred around: nanoparticles and magnetite (Fe<sub>3</sub>O<sub>4</sub>), crystal structure and spectroscopy, oxidation and catalysis, X-ray diffraction (XRD) and Raman spectroscopy, <sup>57</sup>Fe and cathodes, and Co and thin films. In the last 30 years, the number of articles per year that mention the technique has hovered around 1250. More recently, Mössbauer spectroscopy has experienced a great rediscovery, particularly in the industrial sector for the solution of some problems, but also in space exploration.

## KEYWORDS

corrosion, Mars, Mössbauer spectroscopy, phase transition, valence

## 1 | INTRODUCTION

In 1957, Rudolf L. Mössbauer was a promising student of the Technical University in Munich and at the Max-Planck Institute in Heidelberg working on his doctoral thesis under the supervision of professor Maier-Leibnitz. He discovered recoilless emission and absorption of gamma rays from nuclear transitions.<sup>[1–3]</sup> Only a few years later, in 1961, he was awarded the Nobel Prize in Physics at the age of 32 and his discovery took the name

Mössbauer effect. The extraordinary potential of this phenomenon was soon directed to the development of a new type of spectroscopy (Mössbauer spectroscopy, MÖS) that has rapidly contributed to a large number of research disciplines, such as solid state research, physics, chemistry, industry, metallurgy, biology, geology, cultural heritage, archaeology, and planetary exploration (Figure 1).<sup>[4–6]</sup>

MÖS represents a powerful tool to investigate electronic structure, magnetic behaviour, phase transitions, molecular symmetry, and bonding properties of numerous materials.

This is an open access article under the terms of the Creative Commons Attribution License, which permits use, distribution and reproduction in any medium, provided the original work is properly cited.

© 2021 The Authors. The *Canadian Journal of Chemical Engineering* published by Wiley Periodicals LLC on behalf of Canadian Society for Chemical Engineering.



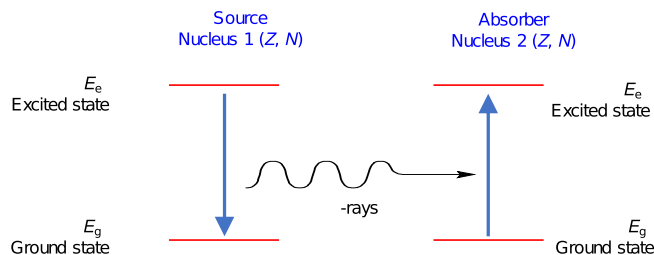


FIGURE 3 Recoilless emission and absorption of gamma rays from nuclear transitions

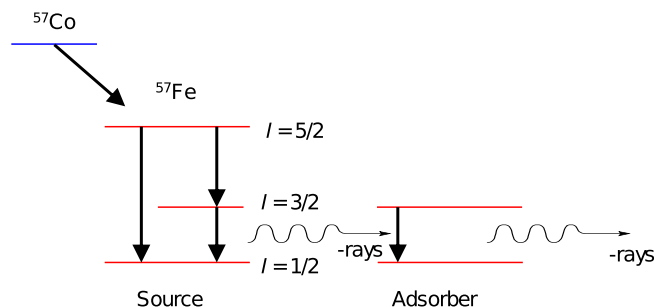


FIGURE 4 (Left) Nuclear decay of  $^{57}\text{Co}$  leading to  $^{57}\text{Fe}$  emitting  $\gamma$ -rays; (right)  $\gamma$ -rays absorption by another nucleus

excited state (136 keV) with nuclear spin quantum number  $I = 5/2$ , that decays to the ground state ( $I = 1/2$ ) directly or through a 14.4 keV energy level ( $I = 3/2$ ; half-life  $\sim 100$  ns) emitting a  $\gamma$ -ray of 14.4 keV, that can be absorbed by an absorber nucleus.

Resonance absorption happens only when the emission and absorption lines overlap. Free atoms or molecules (e.g., liquids or gases) lose energy due to recoil: the nucleus carries away momentum equal to and in the opposite direction of the emitted  $\gamma$ -ray (no resonance is possible). Atoms and molecules in the solid state absorb  $\gamma$ -rays without a corresponding change in momentum and the absorption resonates when the lines overlap—recoilless emission. Mössbauer demonstrated experimentally that cooling the source and the absorber to a temperature close to that of liquid nitrogen, the emitting nucleus was incapable of recoiling by itself. At sufficiently low temperatures, atoms are so tightly bound to each other in the crystal lattice that they are incapable of recoiling.

A typical Mössbauer spectrum consists of a plot of relative energy transmission versus a series of Doppler velocities of the source. In fact, if both the emitter and absorber have an identical local coordination, the Mössbauer spectrum will be a single peak with a Lorentzian line shape (Figure 6A). However, in reality, the source and the absorber have a different local environment, causing a shift of the nuclear energy levels. Even though these energy shifts are very small (neV,  $\mu\text{eV}$ ), they correspond to large changes in

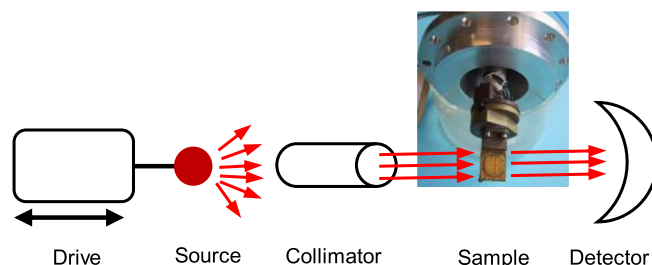


FIGURE 5 Schematic of a Mössbauer spectrometer

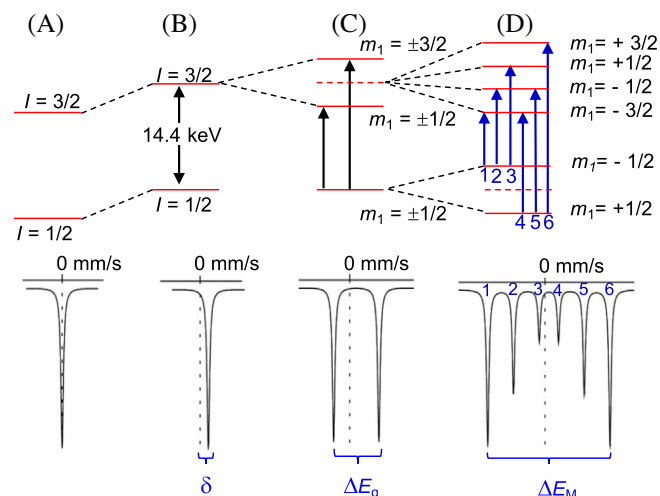


FIGURE 6 Hyperfine parameters observed in Mossbauer spectra: (A) free atom decaying from excited to ground state, (B) isomer shift, (C) electric quadrupole splitting, and (D) magnetic Zeeman splitting

absorbance. To bring the emitter and absorber in resonance, it is necessary to change the gamma ray energy. This is possible by exploiting the Doppler shift.

A conventional Mössbauer instrument consists of a velocity driver that moves a radiation source (typically  $^{57}\text{Co}$ ) generating  $\gamma$ -rays (Figure 5).<sup>[8]</sup> A collimator concentrates the radiation onto a sample that is less than 1 to 5 g (50  $\mu\text{m}$  thick).<sup>[10]</sup> They pass through the sample and reach a NaI(Tl) scintillator detector or  $\text{YAlO}_3(\text{Ce})$ .<sup>[11]</sup> The role of the drive, which is generally a velocity transducer, is crucial because it moves the source in a carefully controlled mode, shifting the energy of the source  $\gamma$ -rays exploiting the Doppler effect. This is necessary in order to allow a partial overlap between emitter and absorber. The velocity of the drive,  $\text{mm s}^{-1}$ , is the conventional unit for the x-axis of Mössbauer spectra.

The detector measures the number of  $\gamma$ -photons as a function of the speed of the drive and the peaks represent the decreased intensity due to the absorption by the sample (in fact the peaks go down in the standard representation of the spectra).

## 2.2 | Hyperfine interactions

Typically, three types of hyperfine interactions can be observed by MÖS that represent the Mössbauer parameters: isomer shift ( $\delta$ ) (Figure 6B), electric quadrupole splitting ( $\Delta E_q$ ) (Figure 6C), and magnetic Zeeman splitting ( $\Delta E_M$ ) (Figure 6D).

From these three parameters, the oxidation state, the mineral phase identity, and in some cases the particle size of a sample, can be determined.

### 2.2.1 | Isomer shift ( $\delta$ )

This parameter is related to Coulomb interactions between protons in the nucleus and neighbouring electrons (mainly s electrons). Although the electronic wave functions cannot overlap with the nucleus, this is not the case for s electrons having a finite probability to penetrate the nuclear volume. The overlap between electrons and nucleus changes the nuclear energy levels, leading to energetic changes in the entire system. This energy variation appears as a shift of the peak with respect to the resonance energy,  $\delta = E_{\text{source}} - E_{\text{absorber}}$  (Figure 6B). The isomer shift relates to the oxidation state of the nucleus, its spin state, and its bonding properties. Figure 7 shows isomer shift expected for iron compounds that differ from oxidation and spin state.

### 2.2.2 | Electric quadrupole splitting ( $\Delta E_q$ )

If at least one of the nuclear states involved in the Mössbauer effect has an electric quadrupole moment ( $I < 1/2$ ) and if at the same time the electric field around the nucleus is heterogeneous (e.g., because of non-cubic distribution of the valence electrons around the nucleus

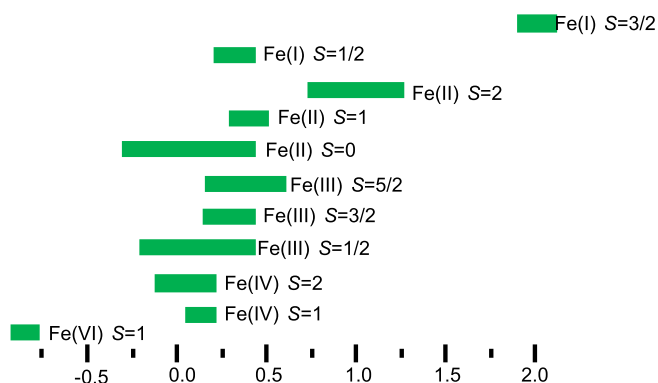


FIGURE 7 Range of isomer shifts in iron compounds differing for oxidation and spin states

and/or non-cubic lattice surroundings), electric quadrupole interactions split the nuclear energy level into two substrates having magnetic quantum number  $m_1 = 3/2$  and  $\pm 1/2$ , respectively (Figure 6C). Figure 8 shows typical quadrupole splitting for three iron complexes.

The Mössbauer spectrum of the low spin complex  $K_4[Fe(CN)_6]$  (Figure 8, top) does not show electric quadrupole splitting thanks to the regular octahedral symmetry of the six CN-ligands allowing the six valence electrons to be organized in a cubic symmetry. The replacement of one of the CN-groups by another type of ligand (e.g., NO) causes a significant distortion of the cubic symmetry, leading to a quadrupole splitting (Figure 8, bottom). In the case of the high spin complex  $[Fe(H_2O)_6]SO_4 \cdot 7H_2O$ , the non-cubic distribution of the six valence electrons is responsible for the quadrupole splitting (Figure 8, middle). In fact, the five d orbitals, split owing to Jahn-Teller distortion, contain the six valence electrons in order to have the lowest orbital occupied by two electrons, whereas the other four orbitals are each occupied by one electron.<sup>[12]</sup>

### 2.2.3 | Magnetic Zeeman splitting ( $\Delta E_M$ )

Zeeman splitting occurs when the nuclear states involved have a magnetic dipole moment and a magnetic field is present at the nucleus. The interaction between the

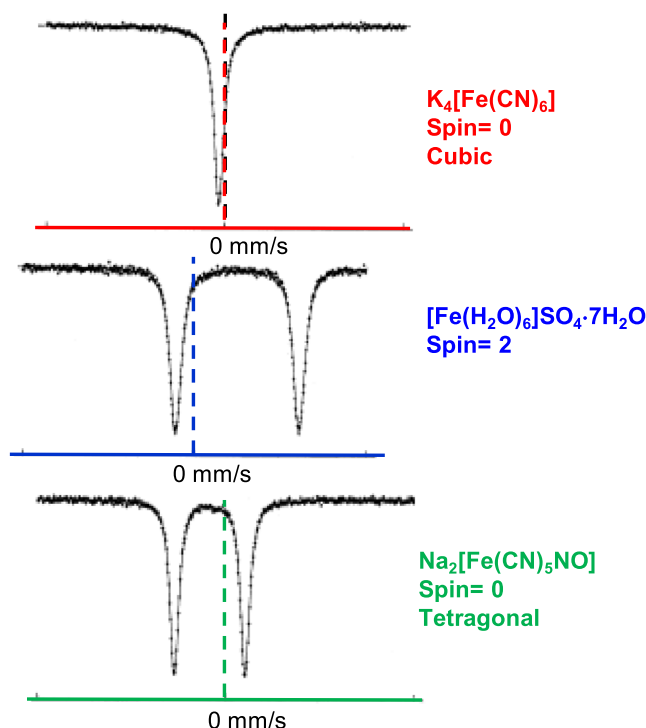


FIGURE 8  $^{57}Fe$  Mössbauer spectrum of three Fe compounds differing for spin and oxidation states

nuclear magnetic dipole and the magnetic field at the nucleus splits the nuclear states having  $I \geq 1/2$  into  $2I + 1$  substates characterized by the magnetic spin quantum numbers  $m_I$ . For a nuclide such as  $^{57}\text{Fe}$ , having a  $I = 1/2$  ground state and a  $I = 3/2$  excited state, this interaction leads to a ground state doublet and an excited state quadruplet. The Mössbauer spectrum is thus magnetically split into a sextet. In the case of a single magnetic dipole interaction, the Mössbauer peaks are equidistant (Figure 6D). This is not true when both magnetic dipole and electric quadrupole interactions are present. In this case, Figure 6D is an approximation. The sublevel structure is more complicated, and the six peaks are not equidistant. When the magnetic interaction is much larger than the quadrupole interaction, the inner four peaks shift to the left and the outer two peaks to the right if the quadrupole interaction is positive (the opposite occurs for a negative quadrupole interaction). The shift of each line is known as the quadrupole shift ( $\epsilon$ ) and is proportional to the electric field gradient at the nucleus.

### 2.2.4 | Magnetically ordered materials

Though the application of an external magnetic field to the sample is often exploited in MÖS, especially to improve the resolution of complex spectra, it is the presence of an internal magnetic field in magnetically ordered (i.e., ferro-, ferri-, or antiferro-magnetic) Mössbauer-active materials that makes MÖS such a powerful technique. This is especially true for the important oxides of Fe, which magnetically order at critical temperatures  $T_c$ , spanning a wide range of temperatures from 950–78 K. Above  $T_c$ , a Fe oxide is paramagnetic and its Mössbauer spectrum typically consists of a quadrupole-split doublet. Below  $T_c$ , the magnetic splitting due to the internal field dramatically splits the spectrum into a sextet. The widely dissimilar temperature dependence of the Mössbauer spectra, caused by magnetic phase transitions, and the considerably different Mössbauer parameters among the Fe oxides, make MÖS a powerful technique to identify, characterize, and quantify the Fe oxides in complex mixtures. For instance, lepidocrocite ( $\gamma\text{-FeOOH}$ ) is paramagnetic at room temperature (20–25°C) and its Mössbauer spectrum consists of a quadrupole-split doublet; it becomes a sextet only below  $T_c = 77$  K, when lepidocrocite becomes magnetically ordered. Conversely, goethite ( $\alpha\text{-FeOOH}$ ) is already antiferromagnetically ordered at room temperature ( $T_c = 400$  K) and its Mössbauer spectrum is a sextet down to 4.2 K. Finally, akaganeite ( $\beta\text{-FeOOH}$ ) is paramagnetic at room temperature, its spectrum displaying two quadrupole-split doublets, but it antiferromagnetically orders when cooled down to ( $\approx 240$  °C) and its

spectrum then consists of a sextet with asymmetric lines. It is thus clear that these three Fe oxides can be easily identified and quantified by collecting Mössbauer spectrum at a few temperatures. When a magnetically ordered Fe oxide is present as small particles ( $< 1 \mu\text{m}$ ), it can be in the superparamagnetic regime, when the magnetization, and hence the internal field, rapidly changes its space orientation due to random thermal motion. In this case, the magnetically split sextet collapses in a quadrupole-split doublet. Since superparamagnetism strongly depends on particle size and temperature, the former can be measured by collecting Mössbauer spectra below  $T_c$ . Finally, MÖS is very sensitive to  $^{57}\text{Fe}$  (and few other isotopes) and insensitive to many elements and isotopes (Figure 2), and this makes MÖS a technique of choice for samples where the Fe oxides are too low in concentration or in crystallinity to be investigated and quantified by X-ray diffraction (XRD).

## 3 | APPLICATIONS

MÖS is an elegant tool that researchers apply in industrial sectors,<sup>[4,13]</sup> biology,<sup>[14]</sup> cultural heritage (art and archaeology),<sup>[15,16]</sup> and so on. In the last 3 years, WoS has indexed 3000 articles that mention the technique, of which one-third were in the category of multidisciplinary materials science.<sup>[17]</sup> Condensed matter physics was ranked second among WoS scientific categories during this period with 555 articles, followed by physical chemistry (545), applied physics (389), and multidisciplinary chemistry (373). Chemical engineering was tenth with 120 articles. Compared to Raman and Fourier transform infrared spectroscopy (FTIR), which grew from 1000 articles per year in the late 1980s and early 1990s to over 20 000 in 2020,<sup>[18,19]</sup> MÖS has stagnated at 1 250 100 ( $n = 30$ ) since 1991. These three techniques address the molecular level changes and reactivity (bottom rows of Figures 9 and 10), but MÖS has been less successful integrating operando versus the other two.<sup>[22]</sup>

VOSViewer online software builds word maps based on bibliometric data indexed by WoS and Scopus. It grouped the 100 most mentioned keywords of the 3000 articles published in 2018, 2019, and 2020 into six clusters (Figure 11). The red cluster has 24 keywords and is centred on nanoparticles (NPs),  $\text{Fe}_3\text{O}_4$ , and microstructure. Crystal structure and spectroscopy were the two most mentioned keywords in the green cluster that had 23 keywords. The blue cluster with almost as many keywords (21) contains FeOx, oxidation, and oxide. The close proximity of FeOx and  $\text{Fe}_3\text{O}_4$  demonstrates that they are closely related even though they assigned to different clusters. Yellow, magenta, and light blue clusters are all

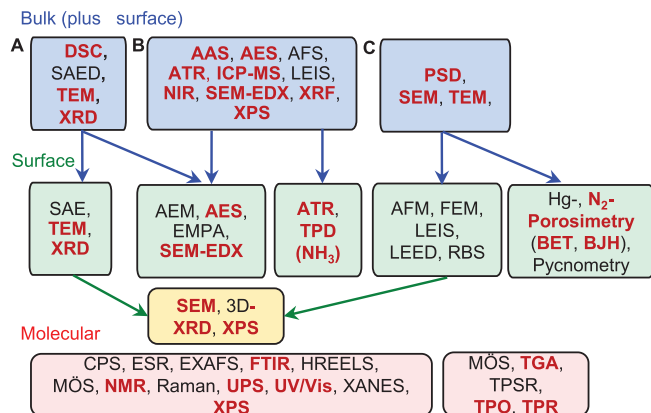


**FIGURE 9** Spectroscopic techniques in catalysis.<sup>[9,20,21]</sup> Class A techniques (left side of the figure) probe the nature of the phases. Class B instruments (centre) measure composition while Class C instruments (right side) assess morphology (Figure 10). MÖS (Mössbauer spectroscopy) straddles all three columns at the molecular level (bottom row), which includes coordination, valence, electronic energy levels, and reactivity. Techniques in **red** are the most frequently applied in *Can. J. Chem. Eng.*<sup>[9]</sup>

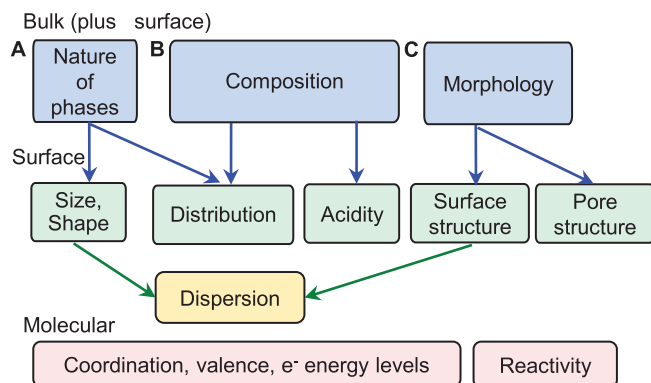


**FIGURE 10** Physico-chemical properties corresponding to the analytical instruments in Figure 9.<sup>[9,20]</sup> Typically, we consider the surface to include up to the first three atomic layers (1 nm, but here several of the analytical techniques, like energy-dispersive X-ray spectroscopy (EDX), penetrate to 1  $\mu\text{m}$ )

closely related as they are concentrated in the same area. XRD, Raman, and FTIR are the most common spectroscopic techniques that researchers apply with MÖS. <sup>57</sup>Fe and Co are the two most common keywords for the yellow cluster and magenta cluster, respectively.

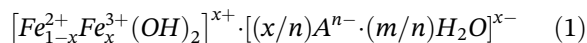
The journals that published the most articles include *Journal of Magnetism and Magnetic Materials* (148 of the 3000 articles), *Journal of Alloys and Compounds* (119), and *Inorganic Chemistry* (92). Of the 3000 articles, the top three cited were related to catalysis: ‘Microporous Framework Induced Synthesis of Single-Atom Dispersed Fe-N-C Acidic ORR Catalyst and Its in Situ Reduced Fe-N4 Active Site Identification Revealed by X-ray Absorption Spectroscopy’

(metal organic frameworks),<sup>[24]</sup> ‘Alumina-Supported CoFe Alloy Catalysts Derived from Layered-Double-Hydroxide Nanosheets for Efficient Photothermal CO<sub>2</sub> Hydrogenation to Hydrocarbons’ (Fischer-Tropsch type reactions),<sup>[25]</sup> and ‘Highly Efficient and Sustainable Non-Precious-Metal Fe-N-C Electrocatalysts for the Oxygen Reduction Reaction’.<sup>[26]</sup> *Applied Catalysis B: Environmental* published some of the most cited articles in the chemical engineering science category: ‘Degradation of Atrazine by Zn<sub>x</sub>Cu<sub>1-x</sub>Fe<sub>2</sub>O<sub>4</sub> Nanomaterial-Catalyzed Sulfite Under UV-Vis Light Irradiation: Green Strategy to Generate SO<sub>4</sub><sup>-</sup>’,<sup>[27]</sup> ‘Methanation of CO<sub>2</sub> on Iron Based Catalysts’,<sup>[28]</sup> and ‘Controlled Formation of Iron Carbides and Their Performance in Fischer-Tropsch Synthesis’.<sup>[29]</sup> Finally, the lively interest in the industrial applications of MÖS is witnessed by the ISIAME (International Symposium on the Industrial Applications of the Mössbauer Effect) conference series, held every 4 years since the early 1980s.

### 3.1 | Mineral identification

MÖS determines valence states (oxidation and spin state), local symmetry, and magnetic properties (Figure 10). Researchers apply it most to differentiate Fe<sup>2+</sup> from Fe<sup>3+</sup> and identify their local coordination from the isomer shift and  $\Delta E_q$ . The technique is nondestructive, which is an advantage compared to conventional analysis of soils and sediments that generally require a strong acid to completely dissolve the matrix before applying a spectrophotometric technique. Thanks to its high sensitivity and selectivity, MÖS identifies traces of iron species in minerals. In some respects, MÖS is similar to X-ray powder diffraction (XRPD) because it produces a fingerprint for each mineral on the basis of the hyperfine parameters ( $\delta$ ,  $\Delta E_q$ , and  $\Delta E_M$ ) but is capable of quantifying amorphous phases undetectable by XRPD.

MÖS contributes to characterizing green rust, which is a mixture of unstable hydroxyl salt minerals<sup>[30]</sup>:



where A<sup>n-</sup> is the intercalated anion (typically SO<sub>4</sub><sup>2-</sup>, CO<sub>3</sub><sup>2-</sup>, and Cl<sup>-</sup>),<sup>[31]</sup> strongly affecting anoxic groundwater and soil horizon. Miniaturized MÖS is capable of measuring oxidation states and the intermediate phases of green rust of the highly unstable complexes in air much better than traditional spectroscopic techniques.<sup>[32-35]</sup> Even though the technique clearly differentiates Fe<sup>2+</sup> from Fe<sup>3+</sup>, because the spectra have two distinct doublet peaks, in reality the high oxygen-sensitivity distorts Fe<sup>2+</sup> and thus Fe<sup>2+</sup>/Fe<sup>3+</sup> and multiple signals appear. However, reducing the experimental



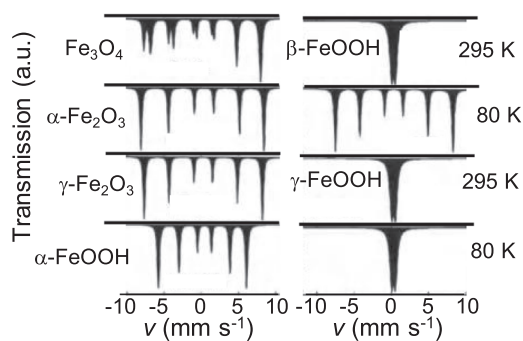


**FIGURE 12**  $^{57}\text{Fe}$  Mössbauer spectra of iron oxides. Left:  $^{57}\text{Fe}$  Mössbauer spectra of iron oxides acquired at 295 K. Right:  $^{57}\text{Fe}$  Mössbauer spectra of  $\beta\text{-FeOOH}$  and  $\gamma\text{-FeOOH}$  acquired at 295 K and at liquid nitrogen temperature (80 K) show the magnetic ordering of the former at  $T > 80$  K. Adapted from Gütlich and García<sup>[39]</sup>

written as  $[\text{Fe}^{3+}]_{\text{tetra}}[\text{Fe}^{2+}\text{Fe}^{3+}]_{\text{octa}}[\text{O}^{2-}]_4$ . Above 850 K ( $T_c$ ), magnetite is paramagnetic and its Mössbauer spectrum can be resolved in a singlet due to the tetrahedral sites and a quadrupole split doublet for the octahedral sites. Below  $T_c$ , magnetite has overlapped sextets related to  $\text{Fe}^{3+}$  ions in tetrahedral sites, and a second one in the superposition of two sextets arising from  $\text{Fe}^{3+}$  and  $\text{Fe}^{2+}$  ions in octahedral sites that are indistinguishable at room temperature because of rapid electron transfer between the two ionic species. Below the Verwey temperature (120 K), the Mössbauer spectrum of magnetite becomes complicated due to the reduction of crystal symmetry.

Haematite,  $\alpha\text{-Fe}_2\text{O}_3$ , is antiferromagnetically ordered below  $T_c = 995$  K. Above  $T_c$ , it has a quadrupole split doublet. At room temperature, the spectrum comprises a sextet. Owing to very small difference in size of the internal magnetic field, the MÖS spectra of  $\alpha$ - and  $\beta\text{-Fe}_2\text{O}_3$  are indistinguishable, but, by adjusting temperature, the oxyhydroxides  $\alpha$ -,  $\beta$ -, and  $\gamma\text{-FeOOH}$  can be identified. In fact, at room temperature  $\alpha\text{-FeOOH}$  (Goethite) displays a magnetically split sextet, whereas  $\beta$ - and  $\gamma\text{-FeOOH}$  show a broad band. However, lowering the temperature down to 80,  $\beta\text{-FeOOH}$  undergoes a magnetic order phase transition showing a split sextet, whereas  $\gamma\text{-FeOOH}$  still exhibits a large broad band. In fact, even lower temperatures are required to magnetically order  $\gamma\text{-FeOOH}$  ( $\sim 30$  K). MÖS is now applied routinely to resolve common industrial corrosion problems, such as identifying finely dispersed particles that form in the cooling systems of power plants.<sup>[13]</sup>

### 3.3 | Discovering Mars

Iron oxide pigment covers most of the surface of Mars and it is widely dispersed in the atmosphere, which

is why it looks red. NASA's researchers equipped Spirit and Opportunity, twin Mars Exploration Rovers, with an MÖS (MIMOS II instrument) to sample Mars' soil to detect traces of water, the basic conditions for life.<sup>[41]</sup> Exploring Meridiani Planum, Opportunity made a very exciting discovery: it recorded the Mössbauer spectrum of the ferric sulphate hydroxide mineral jarosite,  $\text{KFe}_3(\text{SO}_4)_2(\text{OH})_6$ , the best evidence of water on the planet that in the past percolated through the rocks.<sup>[42]</sup> It then demonstrated that at Meridiani Planum, 2% of water in the sedimentary rocks arises from jarosite alone. In the same year on the opposite side of the planet (Columbia Hills) the twin Mars Rover Spirit analyzed the composition of the rocks, discovering a mineral rich in Mg and Fe and poor in Ca that constitutes 16%–34% of the rocks.<sup>[43]</sup> A humid environment rich in  $\text{CO}_2$  can account for high concentration of carbonate in the rock. These discoveries have strongly contributed to increasing the interest of the international scientific community towards exploring the Red Planet, which still represents one of the greatest human challenges.

## 4 | UNCERTAINTY

The accuracy of MÖS analyses is related to four primary independent sources of uncertainty: errors fitting the Mössbauer spectra ( $\sigma_{\text{fit}}$ ), errors associated with the calibration reference materials ( $\sigma_{\text{cal}}$ ), thermal corrections to the spectra because of second order Doppler shift ( $\sigma_{\Delta\delta}$ ), and other experimental errors like assuming a flat background ( $\sigma_{\text{err}}$ )<sup>[44]</sup>:

$$\sigma_{\delta}^2 = \sigma_{\text{fit}}^2 + \sigma_{\text{cal}}^2 + \sigma_{\Delta\delta}^2 + \sigma_{\text{err}}^2 \quad (2)$$

The greatest contribution to uncertainty comes from the complexity of the Mössbauer spectra and degraded spectrum line sharpness. For magnetite nanoparticles (blue cluster and red cluster), the contribution of  $\sigma_{\text{err}}$  to  $\sigma_{\text{delta}}$  was negligible.<sup>[44]</sup> Above 120°C,  $\sigma_{\text{fit}}$  contributes most to the variance while below 120°C,  $\sigma_{\Delta\delta}$  contributes most (Figure 13).  $\sigma_{\text{cal}}$  is insensitive to temperature.

In general, the errors introduced by calibration are negligible compared to other errors: larger contributions come from sample contamination of compounds having similar nuclides, temperature variations during spectra acquisition, and so on. Based on Figure 13, the calculated magnetite content in the samples at each temperature were 4(1)% at 16 K, 5(6)% at 120 K, 41(33)% at 250 K, and 9(6)% at 295 K. Even when constant uncertainty values are reported (0.005 and 0.01  $\text{mm s}^{-1}$ ) and the detection limit for complex Mössbauer spectra is considered to be within a few percent,<sup>[45,46]</sup> in reality numerous other parameters are involved and have to be taken into consideration to minimize approximations.

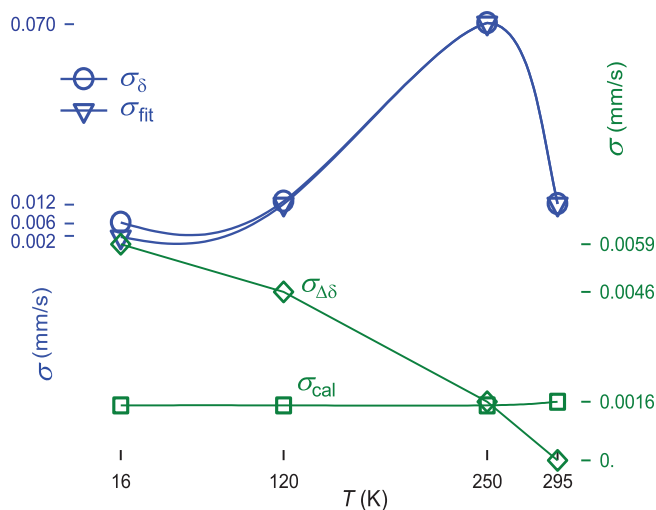


**FIGURE 13** Contributions to the uncertainty as a function of temperature for magnetite nanoparticles.<sup>[44]</sup> The y-axis scale to the left goes with the blue symbols. The y-axis scale to the right goes with the dark green symbols. The lines are trend lines only. The contribution from  $\sigma_{err}$  (Equation (2)) is negligible

MÖS is a sensitive technique thanks to the high energy of the detected  $\gamma$  photons (14.4 keV for  $^{57}\text{Fe}$ ) and the narrow natural linewidth ( $\approx 10^{-8}$  eV), the latter showing that MÖS is also a high-resolution technique. However, MÖS is ill suited for chemical analysis since relating the absorption intensity to the amount of the resonant isotope in the sample involves several parameters (e.g., the recoilless fraction). Thus, the determination of the absolute concentration of a compound by MÖS is hardly possible. Conversely, if several compounds of the resonant isotope are present in a sample, it determines relative amount accurately.<sup>[47]</sup>

We now focus on  $^{57}\text{Fe}$  as the resonant isotope since it is the most investigated and industrially important. The best compromise between sensitivity and reliability of the spectral quantification is achieved using a specimen of areal density  $\approx 10 \text{ mg cm}^{-2}$  of iron, a value that considers the natural abundance (2.14%) of  $^{57}\text{Fe}$ , that is, it refers to all iron isotopes.<sup>[47]</sup> This value corresponds to a thin specimen of solid Fe metal or oxide ( $< 50 \mu\text{m}$ ) or to a millimetre-thick sample containing a few percent of Fe. To the best of our knowledge, a detailed study of the sensitivity of MÖS to the relative amount of the iron phase has not been published. A literature survey of MÖS, as used to quantify iron oxide phases in industrial samples, leads to the reasonable estimate that the sensitivity limit of MÖS to the relative amount of iron oxide phase is  $\approx 5\%$ . In the following, the given percentages all refer to relative amounts. In fine steel corrosion particles formed in the cooling system of a power plant, comprising a complex mixture of six iron oxide phases, 2% of  $\beta/\gamma\text{-FeOOH}$  was detected by

MÖS.<sup>[39]</sup> The MÖS analysis of steel corrosion products in different environments could detect 3% of  $\gamma\text{-FeOOH}$  in samples mainly consisting of  $\alpha\text{-FeOOH}$ .<sup>[48]</sup> In a different context, MÖS was used to analyze samples at different stages of coal production in a South African plant. As low as 10% of jarosite  $[\text{KFe}_3(\text{SO}_4)_2(\text{OH})_6]$  in a sample of as-mined coal and 8% of an unidentified Fe(III)-containing species in coal ash were determined (the coal ash contained just  $0.05 \text{ gg}^{-1}$  of iron oxide). Similar sensitivity was demonstrated in studies of iron-containing natural sediments.<sup>[49]</sup> Finally, an interesting application of MÖS to an element different from iron is the analysis of gold-containing samples from the Fairview BIOX plant in South Africa by  $^{197}\text{Au}$  MÖS. As low as  $\approx 6\%$  (relative amount) of chemically-bound Au was detected after the oxidation stages.<sup>[50]</sup>

## 5 | CONCLUSIONS

MÖS research has reached a plateau of 1000 articles/year over the last two decades, which is an order of magnitude less than nuclear magnetic resonance (NMR), which reached a plateau of 20 000 in 2015.<sup>[51]</sup> In the early days (up to 1975) as many as 70% of the articles mentioned Mössbauer in the title, but this fraction linearly decreased with time to the present-day value of about 20%. This spectroscopic technique is well-established and constitutes a tool for chemical–physical characterization rather than a focal point of research. Interestingly, the relative proportion of these articles is the same since 1985, with physics accounting for more than one-third of the papers, chemistry about one-fourth, and material science about one-fifth—these three fields account for 80% of the MÖS articles. Space research is an exciting field of application, but down on Earth much is concentrated on corrosion and material identification rather than quantification. Another application identifies Fe impurities in Si for electronic and solar panel applications. The measurement error is lowest for magnetite, for example, below 100 K, while the standard deviation exceeds 30% at 250 K.

## PEER REVIEW

The peer review history for this article is available at <https://publons.com/publon/10.1002/cjce.24216>.

## ORCID

Gregory S. Patience  <https://orcid.org/0000-0001-6593-7986>

## REFERENCES

- [1] R. L. Mössbauer, *Z. Phys.* **1958**, 151, 124.
- [2] R. Mössbauer, *Naturwissenschaften* **1958**, 45, 538.
- [3] R. Mössbauer, *Z. Naturforsch.* **1959**, 14a, 211.

- [4] D. Cook, *Hyperfine Interact.* **2002**, 141–142, 21.
- [5] M. Oshtrakh, *Cell Biochem. Biophys.* **2019**, 77, 15.
- [6] R. Dunlap, *The Mössbauer Effect*, Morgan & Claypool Publishers, San Rafael, CA **2019**.
- [7] G. Klingelhöfer, in *Mössbauer Spectroscopy in Materials Science* (Eds: M. Miglierini, D. Petridis), Springer, Dordrecht, The Netherlands **1999**, p. 413.
- [8] M. Dyar, E. Sklute, in *Remote Compositional Analysis: Techniques for Understanding Spectroscopy, Mineralogy, and Geochemistry of Planetary Surfaces* (Eds: J. L. Bishop, J. F. B. III, J. E. Moersch), Cambridge University Press, Cambridge **2019**, p. 147.
- [9] G. S. Patience, *Can. J. Chem. Eng.* **2018**, 96, 2312.
- [10] M. D. Dyar, D. G. Agresti, M. W. Schaefer, C. A. Grant, E. C. Sklute, *Annu. Rev. Earth Pl. Sc.* **2006**, 34, 82.
- [11] A. L. Kholmetskii, M. Mashlan, O. V. Misevich, V. A. Chudakov, A. R. Lopatik, D. Zak, *Nucl. Instrum. Meth. B* **1997**, 124, 143.
- [12] O. A. Yakovleva, *Hyperfine Interact.* **1990**, 56, 1503.
- [13] G. Principi, *Metals* **2020**, 10, 992.
- [14] E. Bill, in *Practical Approaches to Biological Inorganic Chemistry*, 2nd ed. (Eds: R. Crichton, R. Louro), Elsevier, Oxford, UK **2020**, p. 201.
- [15] U. Wagner, F. Wagner, W. Häusler, I. Shimada, in *Radiation in Art and Archeometry* (Eds: D. Creagh, D. Bradley), Elsevier Science B.V., Amsterdam, The Netherlands **2000**, p. 417.
- [16] M. Carbuicchio, R. Ciprian, *Hyperfine Interact.* **2013**, 217, 9.
- [17] Web of Science™ Core Collection 2020, <http://apps.whoofknowledge.com> (accessed: January 2021).
- [18] M. O. Guerrero-Pérez, G. S. Patience, *Can. J. Chem. Eng.* **2020**, 98, 25.
- [19] M. O. Guerrero-Pérez, G. S. Patience, M. A. Bañares, *Can. J. Chem. Eng.* **2021**, 99, 97.
- [20] F. Delannay, B. Delmon, in *Characterization of Heterogeneous Catalysts*, 1st ed. (Ed: F. Delannay), Marcel Dekker, New York **1984**, Ch. 1.
- [21] G. S. Patience, *Experimental Methods and Instrumentation for Chemical Engineers*, 2nd ed., Elsevier B.V., Amsterdam, The Netherlands **2017**.
- [22] J.-M. Jehng, I. E. Wachs, G. S. Patience, Y.-M. Dai, *Can. J. Chem. Eng.* **2021**, 99, 423.
- [23] N. J. van Eck, L. Waltman, *Scientometrics* **2010**, 84, 523.
- [24] M. Xiao, J. Zhu, L. Ma, Z. Jin, J. Ge, X. Deng, Y. Hou, Q. He, J. Li, Q. Jia, S. Mukerjee, R. Yang, Z. Jiang, D. Su, C. Liu, W. Xing, *ACS Catal.* **2018**, 8, 2824.
- [25] G. Chen, R. Gao, Y. Zhao, Z. Li, G. I. N. Waterhouse, R. Shi, J. Zhao, M. Zhang, L. Shang, G. Sheng, X. Zhang, X. Wen, L.-Z. Wu, C.-H. Tung, T. Zhang, *Adv. Mater.* **2018**, 30, 1704663.
- [26] M. Sun, D. Davenport, H. Liu, J. Qu, M. Elimelech, J. Li, *J. Mater. Chem. A* **2018**, 6, 2527.
- [27] Y. Huang, C. Han, Y. Liu, M. N. Nadagouda, L. Machala, K. E. O'Shea, V. K. Sharma, D. D. Dionysiou, *Appl. Catal. B-Environ.* **2018**, 221, 380.
- [28] J. Kirchner, J. K. Anolleck, H. Losch, S. Kureti, *Appl. Catal. B-Environ.* **2018**, 223, 47.
- [29] T. A. Wezendonk, X. Sun, A. I. Dugulan, A. J. F. van Hoof, E. J. M. Hensen, F. Kapteijn, J. Gascon, *J. Catal.* **2018**, 362, 106.
- [30] C. Bender-Koch, S. Mørup, *Clay Miner.* **1991**, 26, 577.
- [31] J. Bernal, D. Dasgupta, A. Mackay, *Clay Minerals Bulletin* **1959**, 4, 15.
- [32] C. Pantke, M. Obst, K. Benzerara, G. Morin, G. OnaNguema, U. Dippon, A. Kappler, *Environ. Sci. Technol.* **2012**, 46, 1439.
- [33] S. Chaudhuri, J. Lack, J. Coates, *Appl. Environ. Microb.* **2001**, 67, 2844.
- [34] J. Miot, M. Etique, in *Iron Oxides: From Nature to Applications* (Ed: D. Faivre), John Wiley & Sons, New York **2016**, p. 53.
- [35] J. Miot, J. Li, K. Benzerara, M. Sougrati, G. OnaNguema, S. Bernard, J.-C. Jumas, F. Guyot, *Geochim. Cosmochim. Ac.* **2014**, 139, 327.
- [36] A. Cuttler, V. Man, T. Cranshaw, G. Longworth, *Clay Miner.* **1990**, 25, 289.
- [37] J.-M. Génin, G. Bourrié, F. Trolard, M. Abdelmoula, A. Jaffrezic, P. Refait, V. Maitre, B. Humbert, A. Herbillon, *Environ. Sci. Technol.* **1998**, 32, 1058.
- [38] D. Latta, M. Boyanov, K. Kemner, E. O'Loughlin, M. Scherer, *Appl. Geochem.* **2012**, 27, 1512.
- [39] P. Gütlich, Y. García, in *Mössbauer Spectroscopy* (Eds: Y. Yoshida, G. Langouche), Springer, Berlin, Germany **2013**, p. 23.
- [40] F. Nagya, Z. Klencsár, *Physics Research Section B* **2006**, 245, 528.
- [41] G. Klingelhöfer, R. Morris, B. Bernhardt, D. Rodionov, P. de Souza Jr., S. Squyres, J. Foh, E. Kankeleit, U. Bonnes, R. Gellert, C. Schröder, S. Linkin, E. Evlanov, B. Zubkov, O. Prilutski, *J. Geophys. Res.-Planet.* **2003**, 108, E12.
- [42] G. Klingelhöfer, R. Morris, B. Bernhardt, C. Schröder, D. Rodionov, P. de Souza, A. Yen, R. Gellert, E. Evlanov, B. Zubkov, J. Foh, U. Bonnes, E. Kankeleit, P. Gütlich, D. Ming, F. Renz, T. Wdowiak, S. Squyres, R. Arvidson, *Science* **2004**, 306, 1740.
- [43] R. Morris, S. Ruff, R. Gellert, D. Ming, R. Arvidson, B. Clark, D. Golden, K. Siebach, G. Klingelhöfer, C. Schröder, I. Fleischer, A. Yen, S. Squyres, *Science* **2010**, 329, 421.
- [44] J. Fock, L. K. Bogart, O. Posth, M. F. Hansen, Q. A. Pankhurst, C. Frandsen, *Hyperfine Interact.* **2016**, 237, 23.
- [45] G. M. da Costa, C. Blanco-Andujar, E. D. Grave, Q. A. Pankhurst, *J. Phys. Chem. B* **2014**, 118, 11738.
- [46] T. P. Almeida, A. R. Muxworthy, T. Kasama, W. W. Wyn, C. Damsgaard, C. Frandsen, T. J. Pennycook, R. E. Dunin-Borkowski, *Geochem. Geophys. Geosy.* **2015**, 16, 2969.
- [47] R. E. Vandenberghe, E. D. Grave, in *Mössbauer Spectroscopy* (Eds: Y. Yoshida, G. Langouche), Springer, Berlin, Germany **2013**, p. 91.
- [48] S. J. Oh, D. C. Cook, H. E. Townsend, *Corros. Sci.* **1999**, 41, 1687.
- [49] E. Murad, J. Cashion, *Mössbauer Spectroscopy of Environmental Materials and their Industrial Utilization*, Springer, New York **2004**.
- [50] J. Friedl, F. E. Wagner, M. D. Adams, R. P. Schouwstra, H. J. Marais, D. Dew, in *XVth CMMI Congress Publications, Vol. 2: Metals Technology and Extractive Metallurgy* (Ed: H. W. Glen), SAIMM, Johannesburg, South Africa **1994**, p. 403.
- [51] M. G. Rigamonti, F. G. Gatti, G. S. Patience, *Can. J. Chem. Eng.* **2019**, 97, 628.

**How to cite this article:** C. L. Bianchi, R. Djellabi, A. Ponti, G. S. Patience, E. Falletta, *Can J Chem Eng* **2021**, 99(10), 2105. <https://doi.org/10.1002/cjce.24216>